

# A Global Analysis of Ion Thruster Plume Interactions for Interplanetary Spacecraft

J. Wang\*, J. Brophy†, and D. Brinza‡

Jet Propulsion Laboratory

California Institute of Technology, Pasadena

## Abstract

A global analysis of ion thruster plume interactions for interplanetary spacecraft is developed based on a fully **3-dimensional** electrostatic **PIC-MCC** model for the near-field region and a **2½-dimensional** electromagnetic hybrid **PIC** model for the far-field region. We show that while the charge exchange ion interaction dominates in the vicinity of the spacecraft, the presence of the solar wind will induce kinetic couplings between the plume and the solar wind in the far-field via electromagnetic plasma instabilities. The instabilities can generate enhanced magnetic field fluctuations leading to wave-particle scattering of both the beam ions and the charge-exchange ions.

## 1. Introduction

Ion propulsion will be used for the first time on an interplanetary spacecraft, Deep Space One (**DS1**) scheduled for launch in July 1998. A primary objective of New Millennium DS1 is to flight validate solar electric propulsion (**SEP**) for interplanetary missions. The cruise phase of the mission will characterize the life and performance of a 30 cm xenon ion thruster and determine how its operation may affect spacecraft payloads and **critical** subsystems.

Effects introduced by the operation of the ion thruster have long raised both technology and science concerns. The technology concerns include plume backflow contamination and spacecraft interactions with the induced **plasma** environment. Backflow contamination can lead to effluent deposition that can **affect** thermal control **surfaces**, optical sensors, solar arrays, science instrumentation, and communications. The induced plasma

environment will modify spacecraft charging characteristics, and can lead to plasma interactions with the solar array. The science concerns relate to plasma measurements. The plume will modify the properties of the solar wind flowing around the spacecraft and may contaminate measurements of the ambient plasma and magnetic fields. As ion thrusters are designed to operate for long periods of time, these effects need to be carefully assessed.

The interactions induced by ion thruster plumes have been studied for some time. Due to the complexity of the problem, the difficulty of matching space conditions in a laboratory, and the lack of opportunities to flight test ion thrusters, computer particle simulations have recently become the best means to study this problem. *Samanta Roy et al.*[1996a,1996b] used hybrid PIC simulations to model the far-downstream region and study charge exchange ion backflow. Wang and *Brophy*[1995] developed full particle and hybrid **PIC-MCC** models of single and multiple thruster plumes and studied the effects of ambient environment on plasma plumes. Wang *et al.*[1996] have carried out 3-D simulations of ion thruster plume environments using parameters similar to those of the NSTAR (NASA Solar-Electric Propulsion Technology Application Readiness) thruster to be used on DS1. All studies on this subject so far have concentrated on charge-exchange ion interactions near the spacecraft. There have been no studies concerning other aspects of plume interactions, such as ion thruster operation in the solar wind environment and plume-solar wind interactions.

For an interplanetary spacecraft such as **DS-1**, the ion thruster operates in the solar wind, which is a tenuous, relatively hot **plasma** with a high flow speed and a frozen-in magnetic field. It is instructive to first review theoretical studies of solar wind interactions with newborn ions related to comets and **collisionless** shocks. Generally speaking there are three mechanisms

\*Member Technical Staff, Advanced Propulsion Technology, Member AIAA

† Supervisor, Advanced Propulsion Technology, Member AIAA

‡ NSTAR Diagnostic Element Lead, Member AIAA

by which newborn ions may interact with solar wind **plasma** and magnetic fields. The first is particle/particle Coulomb collisions which **is** relatively weak due to the low density of the solar wind. The **second** process is cyclotron pickup, in which the **motional** electric field of the solar wind accelerates the newborn ion which then gyrates around a magnetic field line. The third mechanism is scattering of the ions by wave/particle interactions. The consequences of the **collisionless** second and third mechanism are studied in numerous papers for homogeneous plasmas. For instance, **Wu and Davidson[1972]** are among the first to point out that the newly ionized particles in the solar wind can result in collective instabilities that generate **large-amplitude** electromagnetic waves. Gay et **al.[1984, 1986]** presented linear theories and 1-dimensional simulations of **electromagnetic** instabilities driven by a cool ion beam parallel **or** anti-parallel of the solar wind magnetic field. Omid and **Winske[1987]** performed hybrid simulations on the kinetic processes associated with solar wind mass loading due to pickup of cometary ions and the formation of cometary bow shocks. A review of electromagnetic ion/ion instabilities in space **plasmas** is found in **[Gary,1991]**.

Solar wind/ion couplings have never been examined within the context of ion propulsion. In principle, kinetic couplings between the solar wind and new born ions could also occur to an ion thruster plume in the solar wind. However, since the properties of an ion thruster plume are very different from that of cometary ions or cosmic ray particles (for instance, the density of the plume is much larger than that of the solar wind), it is not clear whether any plume-solar wind interactions could occur, and if they can, what the consequences would be.

In this paper we study ion thruster plume interactions in the solar wind. We present an analysis which includes both the near-field ion thruster induced plasma environment and far-field plume-solar wind coupling, We first briefly discuss the properties of the **plasmas** emitted from the NSTAR ion thruster and that of the solar wind in section 2. In section 3, we study plume interactions in the near-field of spacecraft, which establishes the properties of the ion thruster plume. In section 4, we study plume **solar** wind interactions. In particular we investigate whether any plume-solar wind coupling may occur **via collisionless** mechanisms. Section 5 contains a summary and conclusions.

## 2. Ion Thruster Plasma and Solar Wind Plasma

### The Ion Thruster Plasma

In ion thrusters, **propellant** ions are accelerated **electrostatically** by a system of grids to form a high velocity beam; neutralizing electrons are emitted from the neutralizer in conjunction with the beam ions, **Thus** the ion thruster plume is composed of propellant **efflux** (including beam ions, neutralizing electrons, and **neutrals** that escape through the ion optics and from the neutralizer), **nonpropellant efflux** (material sputtered from thruster components and the neutralizer), and a **low-energy** plasma generated through charge-exchange collisions between energetic ions and the neutrals within the plume,

The 30 cm xenon NSTAR thruster to be used on **DS1** has an input power range of 600 to 2500 W. Under typical operating conditions, the beam current is about 1.76 A; and the exit beam velocity is about  $3.5 \times 10^6$  cm/s (beam ion kinetic energy about 1 keV); Near thruster exit, the temperature of beam ions is about **0.04eV** ( $\sim 500$  K), and the temperature of the neutralizing electrons is in the range of 1-5 eV. From these **parameters**, the average beam ion current at thruster exit is  $J_{M0} = I/\pi r_T^2 \simeq 24.9 \text{ A/m}^2$  and the average beam ion density at thruster exit  $n_{b0} = J_{b0}/ev_b \simeq 4.4 \times 10^{19} \text{ cm}^{-3}$ . The propellant ions form a divergent beam with a divergence half angle about 15 to 20° due to the curvature of the thruster exit surface. The radial beam current density profile may be **assumed** to follow a Gaussian distribution, although the actual distribution may be more peaked at the center.

The propellant that remains unionized flows out of the thruster exit in free molecular flow at thermal speeds corresponding to the thruster wall temperature ( $\sim 500$  K). The density of the neutral plume near the thruster exit is about  $10^{12} \text{ cm}^{-3}$  and remains quasi-steady due to the low charge-exchange collision rate. For  $v_b \simeq 3.5 \times 10^4 \text{ m/s}$ , we find that the charge-exchange collision cross section  $\sigma_{ce} \simeq 3.5 \times 10^{-15} \text{ cm}^2$ . Hence, at thruster exit, we find the **charge-exchange** ion production rate  $\frac{dn_{ce}}{dt} \simeq 2.4 \times 10^{13} \text{ cm}^{-3} \text{ s}^{-1}$ . In addition to these propellant and charge-exchange ions a very **small** amount of neutrals may also undergo photoionization or charge-exchange ionization in the solar wind.

### The Solar Wind Plasma

The **solar** wind is a tenuous, relatively hot plasma which flows radially outward from the sun, Since the magnetic field is approximately “frozen” in the conducting solar wind, the solar magnetic field is convected out into space by the solar wind. The expansion of the **solar** wind **plasma** across the interplanetary magnetic field also induces a **motional** electric field in the reference frame at rest with respect to the Sun,  $\vec{E}_0 = -\vec{v}_{sw} \times \vec{B}_0$ . In the reference frame of the solar wind,  $\vec{E}_0 \simeq 0$ . The

solar wind parameters may undergo substantial variation, but typical values are: solar wind density ( $n_w \sim 1 \text{ cm}^{-3}$ ), solar wind flow speed ( $v_w \sim 350 \text{ km/s}$ ), solar wind ion temperature ( $T_i \sim 10 \text{ eV}$ ), and solar wind magnetic field magnitude ( $B_o \sim 10 \text{ nT}$ ). Modest variations in these parameters should not correspond to qualitative changes in the solar wind interaction with the ion thruster plume. In contrast, the angle between the solar wind flow velocity  $\vec{v}_w$  and the interplanetary magnetic field  $\vec{B}_o$ ,  $\alpha$ , can vary from  $0^\circ$  to  $90^\circ$  and is a crucial parameter in much of the physics involved.

### 3. Near-Spacecraft Plume Environment

We first review ion thruster plume interactions near the spacecraft. As the solar wind density is about  $1 \text{ cm}^{-3}$ , it is appropriate to neglect the solar wind plasma as a first approximation. Under the solar wind magnetic field, the gyroradius for the beam ions and the charge exchange ion is much larger than the size of the spacecraft. Hence, the solar wind magnetic field can also be neglected for the near-field region. Thus, the interaction is electrostatic.

During normal ion thruster operation, electron emission keeps the exhaust plume quasineutral and prevents the spacecraft from charging up significantly. Typically the spacecraft potential  $\Phi_s/c$  is much lower than that of the beam ion kinetic energy,  $|e\Phi_s/c| \ll K E_{bi}$ . In the absence of an external electromagnetic field, the beam ions follow nearly line-of-sight trajectories because the electric field within the plume is too small to perturb their motion. Hence, the core region of the ion beam will keep its coherent structure. The electrons are much more mobile than ions, so the center of the plume has a positive potential. This potential causes the slowly moving charge-exchange ions to move transversely out of the plume.

Wang *et al.* [1995,1996] have developed a fully three-dimensional hybrid particle-in-cell with Monte Carlo collision model of the near-field plume environment. In this model, the ions are represented by individual super-particles and the electrons are assumed to have a fluid response in which the density is given by the Boltzmann distribution. A typical simulation setup is shown in Fig. 1a. The spacecraft is modeled as a 3-dimensional box structure with a conducting surface and a surface potential  $\Phi_w$  relative to the ambient. At each time step, the propellant ions are injected into the simulation domain from the thruster exit to form a beam described by

$$|J_{bi}| \simeq J_{bimax} \exp(-(r/r_T)^2) \quad r \leq r_T$$

The initial beam divergent half angle is taken to be about  $15^\circ$ . The neutral plume is treated as a steady state background produced by a free molecular flow. A Monte Carlo representation of particle collisions is utilized to model the charge-exchange collision between the beam ions and the neutral background. The charge-exchange ions are generated according to

$$\frac{dn_{cei}}{dt} = n_{bi} n_n v_{bi} \sigma_{cei}(v_{bi}) \quad (1)$$

based on the beam ion and neutral density profile. The trajectory of each charged particle is integrated from

$$\frac{d\vec{m}\vec{V}}{dt} = \vec{F} = q(\vec{E} + \vec{V} \times \frac{\vec{B}}{c}), \quad \frac{d\vec{x}}{dt} = \vec{V} \quad (2)$$

using a standard leapfrog scheme, and the self-consistent electric field is obtained from the Poisson's equation

$$\nabla^2 \Phi = -4\pi\rho \quad (3)$$

Since computationally it is not feasible to set the simulation domain large enough for the outer boundary to be the undisturbed ambient, a Neumann condition  $\nabla\Phi_n = 0$  is used at all outer boundaries of the simulation domain.

Some typical simulation results are shown in Figs. 2 and 3. For this simulation, the spacecraft is taken to be a cubic box with dimension  $1\text{m} \times 1\text{m} \times 1\text{m}$ . The spacecraft is located at  $2 \leq x \leq 16$ ,  $15 \leq y \leq 29$ , and  $15 \leq z \leq 29$ . The thruster exit center is located at  $x = 18$ ,  $y = 22$ , and  $z = 22$ . The thrust direction is in the  $x$  direction. The grid resolution is taken to be  $d_{cell} \simeq 5.2\text{cm}$ . The spacecraft potential is taken to be  $\Phi_s/c/T_e \simeq -3$ . Fig.2 shows the contours of potential and the total ion density and the vectors of the charge-exchange ion current density on a  $xy$  plane cutting through the spacecraft and thruster center. Fig.3 shows contours of the charge exchange ion density on a  $xy$  plane cutting through different  $z$  locations. We find that the outflow of the charge-exchange ions forms a wing-shaped structure. Once outside the plume, the charge-exchange ions come under the influence of the potential of the spacecraft sheath. As the spacecraft potential is typically negative, these ions will therefore be drawn back to the spacecraft.

### 4. Far-Field Plume-Solar Wind Interactions

#### Formulation and Approach

We next consider ion thruster plume in the solar wind plasma. The global scale plume-solar wind interaction is illustrated in Fig.1b. For convenience, we choose a

reference frame moving with the **solar** wind, Hence the solar wind sees a plume move with a relative velocity  $-\vec{v}_{sw} + v_{plume}$ . As  $\vec{v}_{sw}$  is much larger than the beam ion velocity, the relative drift velocity between the solar wind and the plume is dominated by the solar wind flow **speed**. Hence, we do not need to distinguish between the beam ions and the charge-exchange ions. Since our emphasis is on the consequences of the **collisionless process**, we shall consider a **2½-dimensional** (2 spatial components, three velocity and field components), homogeneous model shown in the right corner of **Fig.1b**. We take the relative velocity  $\vec{v}_{dx} = -\vec{v}_{sw} + \vec{v}_{plume}$  along the x direction, and the angle between x and the solar wind magnetic field to be  $\alpha$ . Initially, the solar wind protons follow a **Maxwellian** distribution with a temperature of **10eV** and the plume ions follow a drifting **maxwellian** distribution centered around  $\vec{v}_{dx}$  with a temperature of .04ev.

The plume-solar wind interaction has very **different** characteristics **from** the near-field plume-spacecraft interaction. While the plume-spacecraft interaction is electrostatic in nature, the couplings between the plume ion and **the** solar wind is electromagnetic in nature. While the plume-spacecraft interaction occurs in the vicinity of the spacecraft, the **plume-solar** interaction would occur at a global scale. This is because, if any solar wind/ion coupling could occur, the characteristic electromagnetic wave length would be much larger than the spacecraft size. Hence, our approach differs from that discussed in section 3.

**Our approach is based on electromagnetic hybrid particle** simulation [ *Winske and Omid,1993*]. Since the interactions only concern the ion dynamics, the basic assumptions in our approach are a) the electrons are a **massless** fluid  $m_e = 0$  while the ions are treated as test particles, and b) the displacement current  $\frac{\partial \vec{E}}{\partial t}$  can be neglected in Ampere's law (for low frequency **waves**). Since we concern a **quasineutral** plasma in a global region, quasineutrality is **assumed**. Therefore, the governing equations are

1) **Quasineutrality:**

$$n_e = n_i \quad (4)$$

2) Maxwell's equations in the low frequency approximation:

$$\nabla \times \vec{B} = \frac{4\pi}{c} \vec{J} \quad (5)$$

$$\nabla \times \vec{E} = \frac{\partial \vec{B}}{\partial t} - \frac{1}{c} \quad (6)$$

$$\nabla \cdot \vec{B} = 0 \quad (7)$$

3) The electron fluid equation in the limit of  $m_e = 0$ :

$$\frac{\partial n_e m_e \vec{V}_e}{\partial t} = -en_e(\vec{E} + \vec{V} \times \frac{\vec{B}}{c}) - \nabla \cdot \mathbf{P}_e + en_e \mathbf{R} \cdot \vec{J} \quad (8)$$

where the electron pressure tensor is given by:

$$\mathbf{P}_e = n_e T_e \mathbf{I} \quad (9)$$

and the **resistivity** tensor  $\mathbf{R} = \eta \mathbf{I}$  describes short wavelength, high frequency wave-particle interactions not explicitly included in the hybrid model.

4) Dynamic equation for individual ion particles

$$m_i \frac{d\vec{v}_i}{dt} = \vec{F} = q(\vec{E} + \vec{v}_i \times \frac{\vec{B}}{c}) - q\eta \vec{J}, \quad \frac{d\vec{x}_i}{dt} = \vec{v}_i \quad (10)$$

## Results and Discussions

In the simulations presented here we consider two flow conditions, the parallel flow ( $\alpha = 0^\circ$ ) and the perpendicular flow ( $\alpha = 90^\circ$ ) conditions. We take the plume to solar wind density ratio to be  $n_X/n_{sw} \sim 100$ .

The simulation **results** are presented in Fig.4 through Fig.10. Due to computational limitations, an artificial proton mass of  $m_p/m_X = 16$  is used. This compresses the relative plume ion and solar wind proton gyroperiods but does not affect the qualitative picture of the physics. In the solar wind reference frame, the relative plume velocity normalized by the **Alfven** speed for the plume ions,  $v_{AX} = B_0/\sqrt{4\pi n_X m_X}$ , is  $v_{AX}/v_{AX} \approx 63.2$ .

**The velocity distributions for the plume ions and the solar wind protons for the  $\alpha = 0^\circ$  case are shown in Figs. 4 and 5, respectively.** The distribution functions are shown for  $t\Omega_X = 0, 8, 16, 24, \text{ and } 48$ . We find that the solar wind-plume coupling shows a two stage **process**. In the first **stage** ( $t\Omega_X \leq 8$ ), the velocity distributions for the plume ion show little change. However, the distribution functions for the solar wind protons have changed from an isotropic **Maxwellian** distribution to a drifting **Maxwellian** with a **drifting** speed about  $0.16v_{AX}$  along the x direction. This indicates that the solar wind protons are partially "picked up" by the plume. However, in the second stage, the plume ions start to lose their **drifting** speed and **thermalize**. At  $t\Omega_X \geq 48$ , we find that the plume ions have completely **thermalized** into a isotropic distribution. In other words, in the reference frame of the sun, the plume ions are swept away by the solar wind as a warm cloud. Hence, the plume has lost its original properties

The velocity distribution functions for the  $\alpha = 90^\circ$  case are shown in Figs. 6 and 7. The plume ions behave similarly to that for the  $\alpha = 0^\circ$  case, although the

**thermalization** starts a little later, The **solar** wind protons **settle** to a drifting distribution with a **drifting** speed about  $0.19v_{dX}$  during the **first** stage. During the second stage, the relaxation process is **slower** in the direction parallel to  $\vec{B}_0$ .

To understand these results, we analyze the time **history** of the plume ion energies associated with the three velocity components and the magnetic wave energy density in the system  $((\delta B/B_0)^2)$  (Figs. 8 and 10). For the  $\alpha = 0^\circ$  case, we find that the magnetic wave energy start to grow exponentially at  $t\Omega_X \sim 15$ , indicating an electromagnetic instability is excited. As the instability grows, wave-particle interactions drive the system toward isotropy and reduces the amount of free energy available for wave growth, Hence, the growth of wave energy is accompanied by a decrease of  $v_x$  and **increases** in  $v_y$  and  $v_z$ . The wave energy saturates at an almost constant level at  $t\Omega_X \simeq 40$ . The fact that  $(\delta B/B_0)^2 \gg 1$  after instability excitation suggests that the wave-particle interaction is strongly non-linear. For the  $\alpha = 90^\circ$  case, the time histories have similar **characteristics**. However, the magnetic field fluctuations is only **about** 40% of that for  $\alpha = 0^\circ$ . This **indicates** that the instability is weaker in the  $\alpha = 90^\circ$  case.

We also carry out a Fourier **frequency** analysis of the magnetic field fluctuations. Figs. 9 and 11 show the power spectra of the three magnetic field components for the  $\alpha = 0^\circ$  and  $\alpha = 90^\circ$  cases, respectively. For the  $\alpha = 0^\circ$  case, the spectra shows a strong enhancement of transverse magnetic fluctuations at frequencies  $\omega_r \sim 0.5\Omega_X \ll \Omega_p$ . However, the spectra for  $\alpha = 90^\circ$  have two peaks, one at  $\omega_r \sim 0.5\Omega_X$  and the other at  $\omega_r \sim 2\Omega_X$ . The spectra for  $\alpha = 90^\circ$  suggest that the fluctuations arise **predominantly** from cyclotron **resonance** in this case.

We have also performed simulations for  $n_x/n_w = 10$  and  $n_x/n_w = 1000$ . The  $n_x/n_w = 10$  case shows an earlier instability excitation while the  $n_x/n_w = 1000$  case shows a much later instability excitation.

The physics of the **collisionless** plume ion-solar wind coupling can be summarized as follows. Under the perpendicular flow condition,  $\alpha \sim 90^\circ$ , cyclotron pickup leads to a ring-shaped newborn ion velocity distribution. Under the parallel flow condition,  $\alpha \sim 0^\circ$ , there are no magnetic forces on the newborn ions and the resulting distribution is a beam moving along the background magnetic field relative to the solar wind distribution. If  $\alpha$  has an intermediate value, the newborn ions assume a ring-beam distribution. These **non-Maxwellian** distributions **represent** a strong source of free energy relative to the solar wind ion velocity distribution, and can excite a variety of instabilities which lead to en-

hanced fluctuations which, in turn, scatter the plume ions toward **isotropization**[*Gary,1991*].

## 5. Summary and Conclusions

We have developed a global analysis of ion thruster plume interactions for interplanetary spacecraft which includes a fully 3-dimensional electrostatic **PIC-MCC** model for near-field interactions and a **2½-dimensional** electromagnetic hybrid **PIC** model for far-field **plume-solar** wind couplings. We show that different physical process dominates in different plume regions. In the near-field region of the spacecraft, the interaction is driver by the low energy charge-exchange ions responding to the electrostatic potential. The presence of the **solar** wind environment may induce complex plume-solar wind interactions. In the vicinity of the thruster, since the thruster plume will dominate the spacecraft environment due to their much higher density, the main effect of the plume is simply to modify the solar wind **as** it flows past the plume region. However, far away from the thruster where the plume density **has** decreased to a level that the solar wind plasma and fields can penetrate the plume, we find that the plume ions may couple with the solar wind through collective plasma effects. This is because both the low energy **charge-exchange** ions and the energetic beam ions, constitute a free energy source, which may drive one of several electromagnetic instabilities. The instabilities can generate enhanced magnetic field fluctuations, leading to significant particle scattering. This wave particle scattering **will modify the properties of both the solar wind and the plume**. Due to the large amount of free energies carried by the plume, the wave-particle interactions are highly non-linear, and can scatter the beam ions and charge-exchange ions into a isotropic distribution in the solar wind reference frame. This raises the possibility that far-field interactions may affect the plasma environment in the vicinity of the spacecraft. The scenario for maximum **plume-solar** wind coupling would be for the ion thruster to thrust in the direction anti-parallel to the local solar wind flow direction.

The far-field analysis presented in this paper only addresses the possibility and the mechanisms of solar **wind-plume interactions** but does not attempt to quantify the effects of far-field interactions on the near-field environment. The homogeneous model also does not address the effects of finite plume size which inhibits growth of the electromagnetic instabilities. These issues will be addressed in our future work, which will extend this study to 3-D hybrid electromagnetic simulations to resolve plume-solar wind coupling in a global interaction region,

## Acknowledgement

We would like to thank **Dr. S.P. Gary** (Los Alamos National Lab) for many useful **discussions**. This work was carried out by the Jet Propulsion Laboratory, California Institute of Technology under a contract with NASA. **Access** to the Cray **supercomputers** used in this study **was** provided by funding from NASA Offices of Mission to Planet Earth, Aeronautics, and Space **Science**.

## References

- [1] **S.P. Gary**, C. Smith, M. Lee, M. Goldstein, D. **Forslund**, Electromagnetic ion beam instabilities, *Phys. Fluids*, 28, 1984, pp438
- [2] **S.P. Gary**, C. Madland, D. **Schrivver**, and D. **Winske**, computer simulations of electromagnetic cool ion beam instabilities, *J. Geophys. Res.*, 91(A4), 1986, pp4188.
- [3] **S.P. Gary**, Electromagnetic ion/ion instabilities and their consequences in space **plasmas**: a review, *Space Sci. Reviews*, 56, 1991, pp373.
- [4] Omid and Winske, A kinetic study of solar wind **mass** loading and cometary bow shocks *J. Geophys. Res.*, 92(A12), 1987, pp13409.
- [5] R. **Samanta Roy**, D. Hastings, and N. **Gatsonis**, Ion-thruster modeling for backflow contamination, *J. Spacecraft Rockets*, 33(4), 1996a, pp525.
- [6] R. **Samanta Roy**, D. Hastings, and N. **Gatsonis**, Numerical study of spacecraft contamination and interactions by ion-thruster effluents, *J. Spacecraft Rockets*, 33(4), 1996b, pp535.
- [7] D. **Winske** and N. Omid, Hybrid codes, methods and applications, in *Computer Space Plasma Physics: Simulation Techniques and Software*, edited by H. Mataumoto and Y. **Omura**, Tokyo, 1993.
- [8] J. Wang and J. **Brophy**, 3-D Monte-Carlo **particle**-in-cell simulations of ion thruster plasma interactions, *AIAA Pap.* 95-2826, 1995.
- [9] J. Wang, J. **Brophy**, and D. **Binza** 3-D simulations of NSTAR ion thruster plasma environment, *AIAA Pap.* 96-9202, 1996.
- [10] C. Wu and R. Davidson, Electromagnetic instabilities produced by neutral-particle ionization in interplanetary Space, *J. Geophys. Res.*, 77(28), 1972, pp5399.

## Figure Captions

Figure 1: Model setup. a) Near-field interaction model. b) Far-field interaction model.

Figure 2: **Plasma** plume on a xy plane cutting through the center of thruster and spacecraft. a) **Potential** contours. b) Total ion density contours (contour level:  $n_{ion}/n_{bio} = 10^{-4}, 5 \times 10^{-4}, 10^{-3}, 5 \times 10^{-3}, 10^{-2}, 5 \times 10^{-2}, 0.1, 0.5, 1., 1.5$ ). c) Charge-exchange ion current vectors  $J_{ce\pm}$ .

Figure 3: Charge-exchange ion density contours on a xy **plane** cutting through different z locations: z = 24 (a), z = 25 (b), and z = 28 (c).

Figure 4: Plume ion velocity distributions for the  $\alpha = 0^\circ$  case. The distributions are plotted at  $\Omega_x t = 0$  (solid), 8 (dashed), 16 (dotted), 24 (dot-dashed), and 48 (dot-dot-dashed).

Figure 5: Solar wind proton velocity distributiona for the  $\alpha = 0^\circ$  case. .

Figure 6: Plume ion velocity **distributions** for the  $\alpha = 90^\circ$  **case**. The distributions are plotted at  $\Omega_x t = 0$  (solid), 8 (dashed), 16 (dotted), 24 (dot-dashed), and 48 (dot-dot-dashed).

Figure 7: Solar wind proton velocity distributiona for the  $\alpha = 90^\circ$  case.

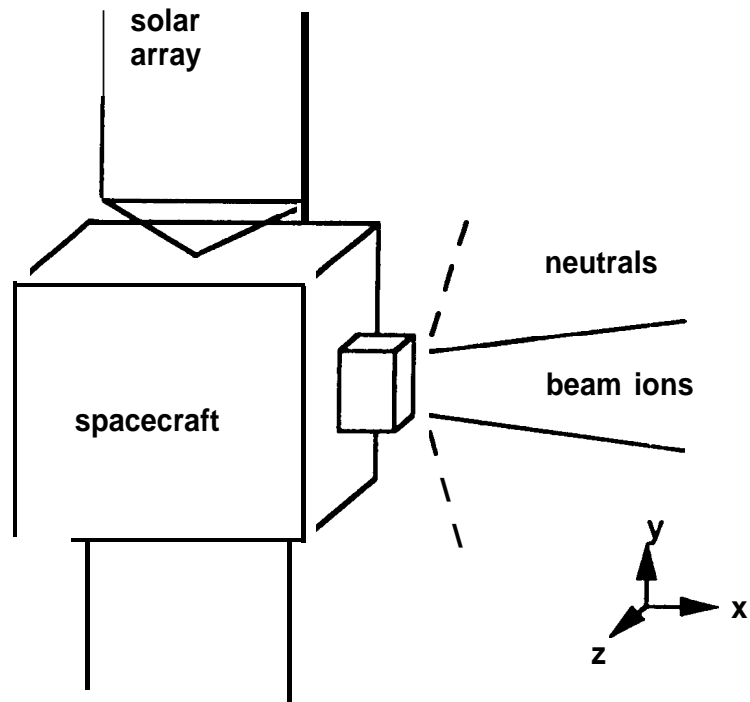
Figure 8: Time histories for the  $\alpha = 0^\circ$  case. a) magnetic field fluctuation energy density  $\delta B^2/B_0^2$ . b) plume ion energy densities  $\frac{v_j^2}{2v_{Ax}^2}$  (j = z: solid line; j = y: dashed line; j = x: dotted line.)

Figure 9: Fourier frequency spectra for the  $\alpha = 0^\circ$  **case**. ( $|\delta B_x|^2$ : solid line;  $|\delta B_y|^2$ : dashed line;  $|\delta B_z|^2$ : dotted line.)

Figure 10: Time histories for the  $\alpha = 90^\circ$  **case**. a) magnetic field fluctuation **energy** density  $\delta B^2/B_0^2$ . b) plume ion energy densities  $\frac{v_j^2}{2v_{Ax}^2}$ . (j = x: solid line; j = y: dashed line; j = z: dotted line.)

Figure 11: Fourier frequency spectra for the  $\alpha = 90^\circ$  **case**. ( $|\delta B_x|^2$ : solid line;  $|\delta B_y|^2$ : dashed line;  $|\delta B_z|^2$ : dotted line.)

a)



b)

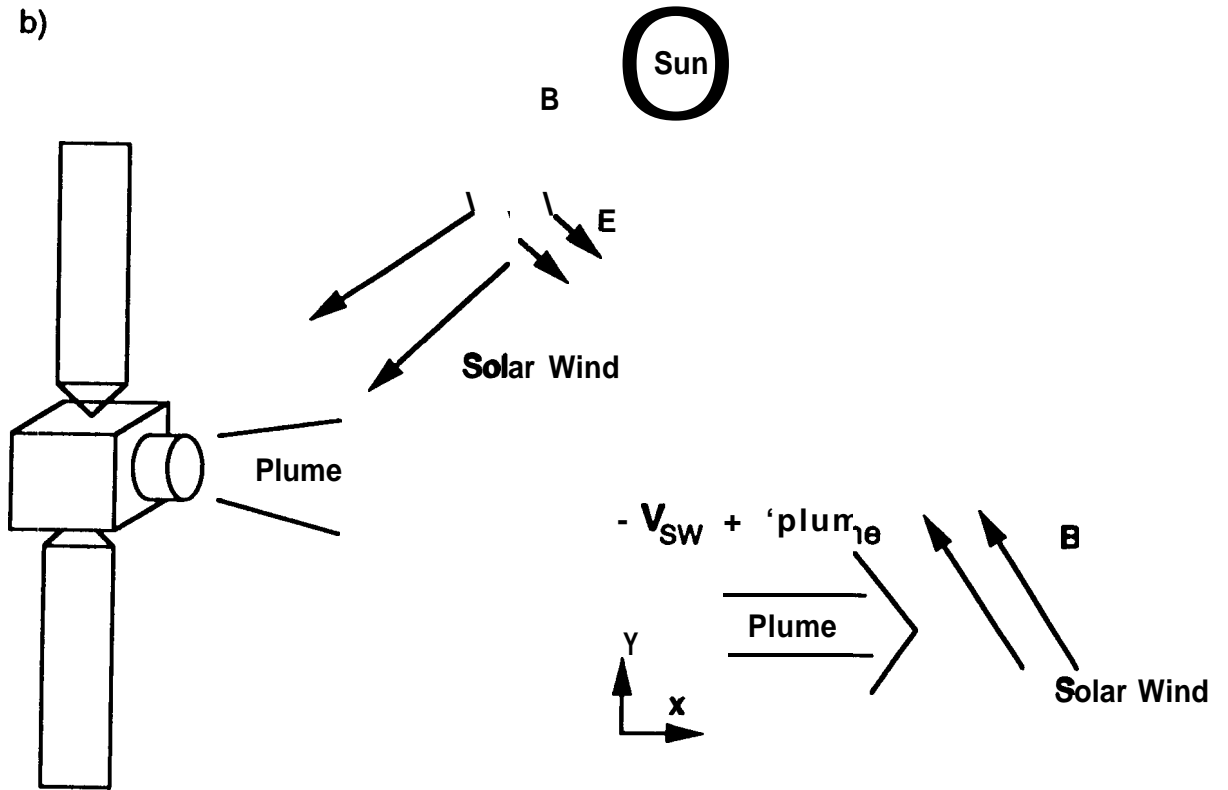


Figure 1

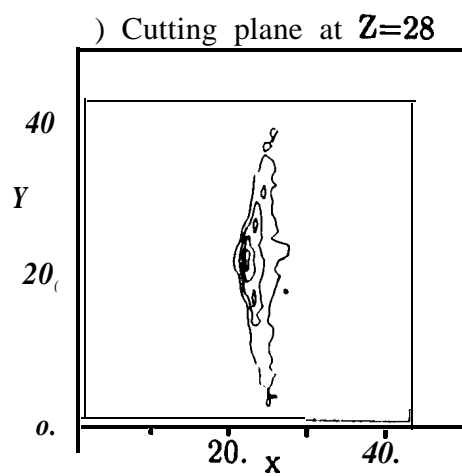
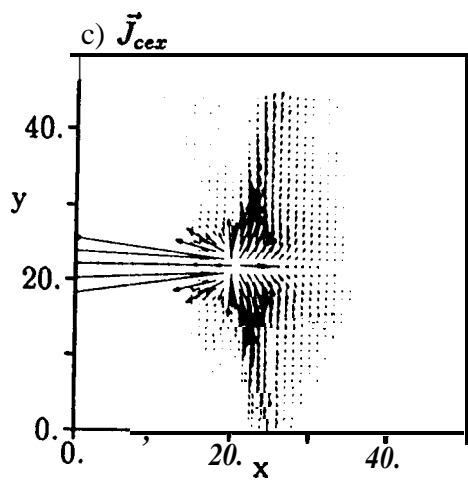
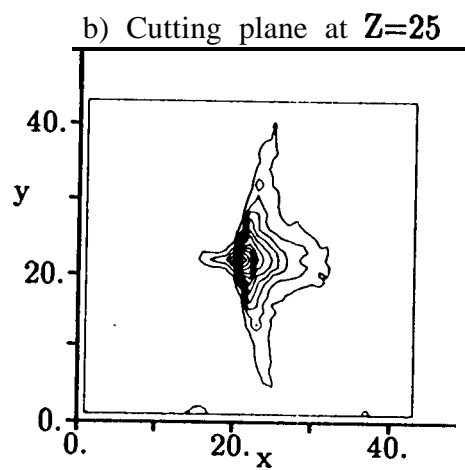
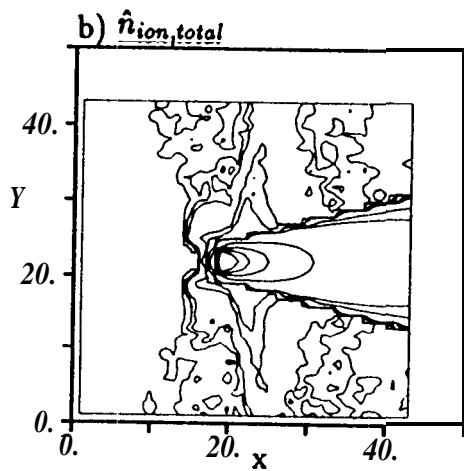
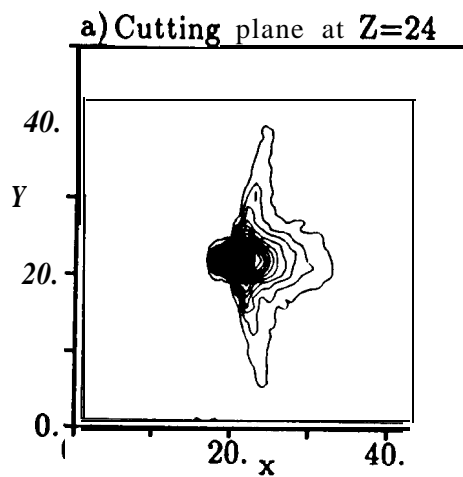
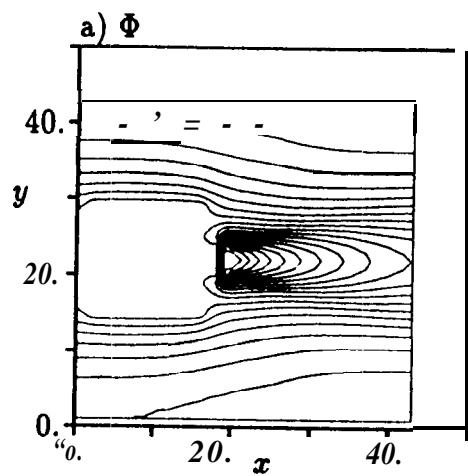


Figure 2

Figure 3

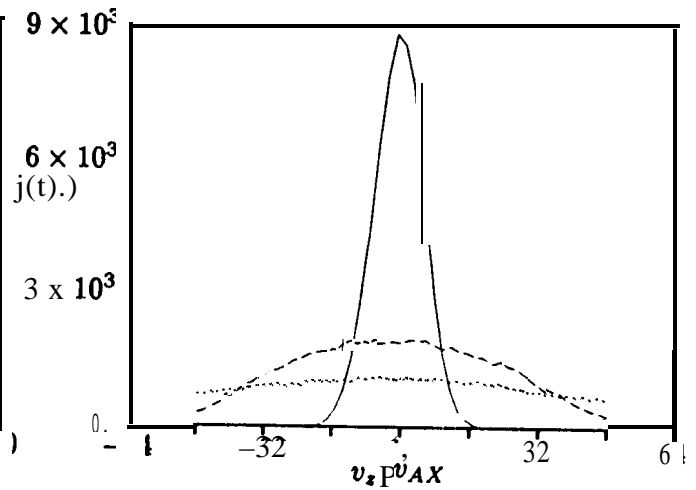
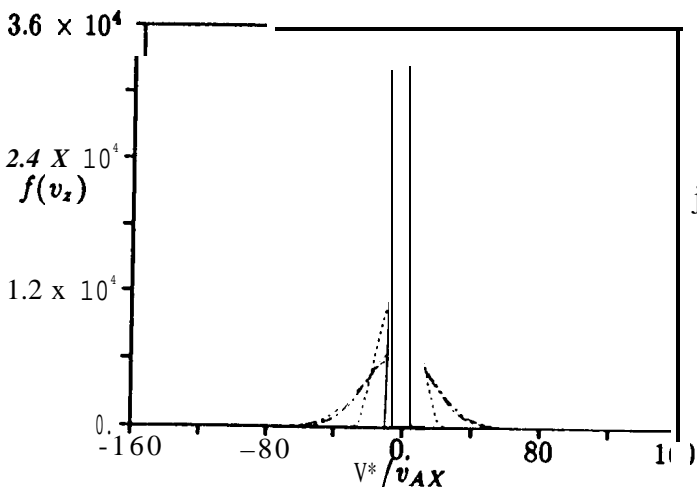
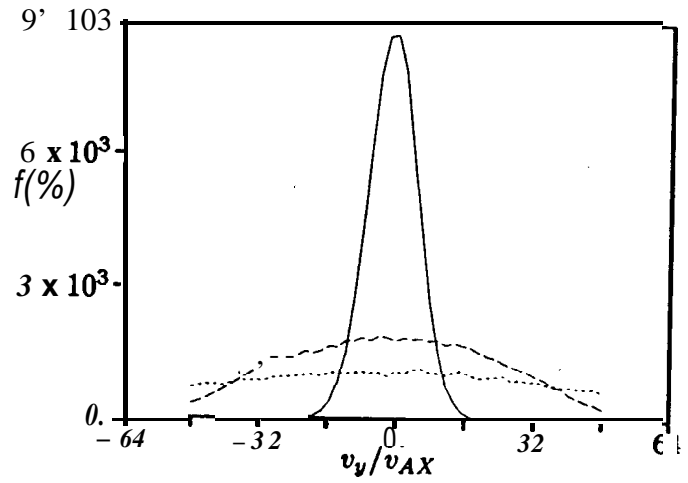
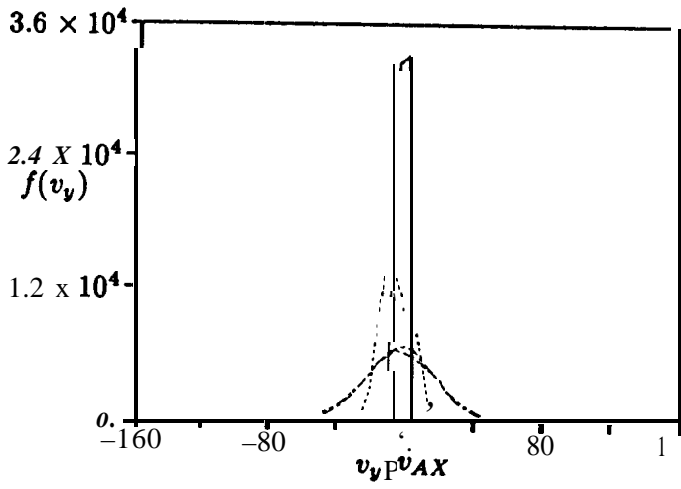
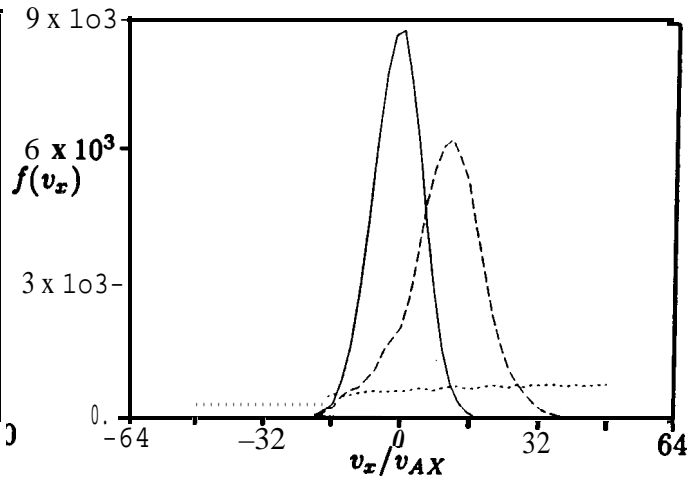
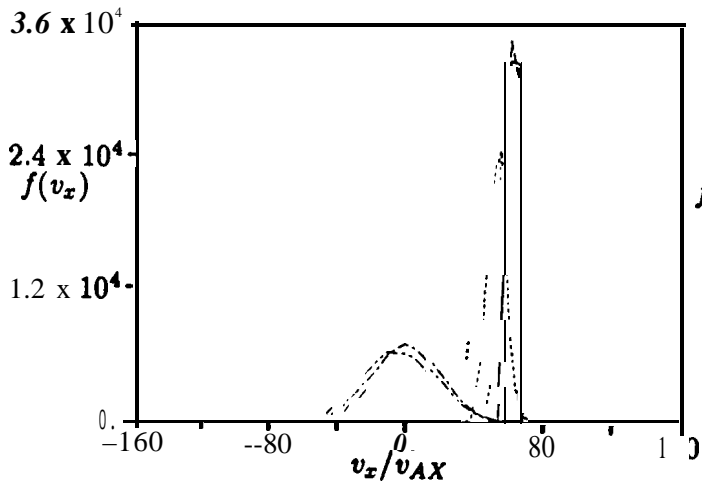


Figure 4

Figure 5

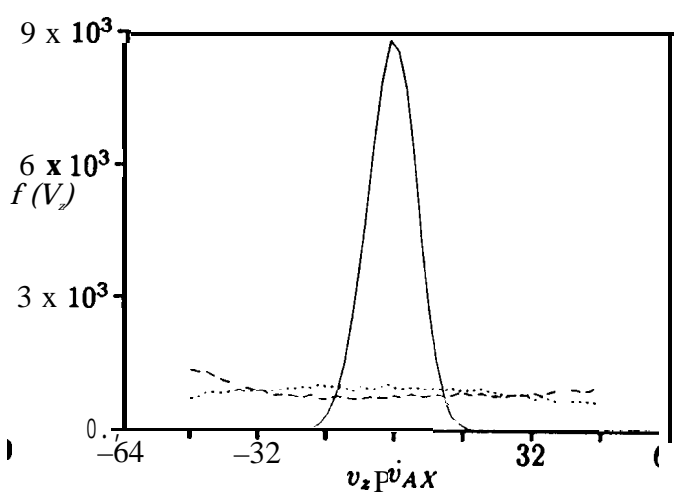
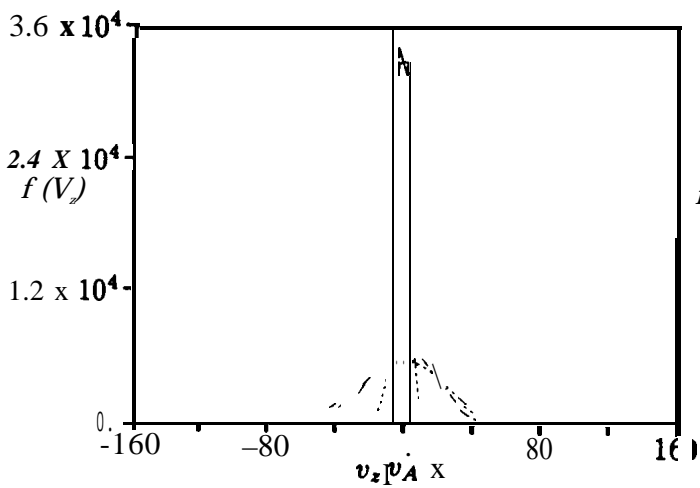
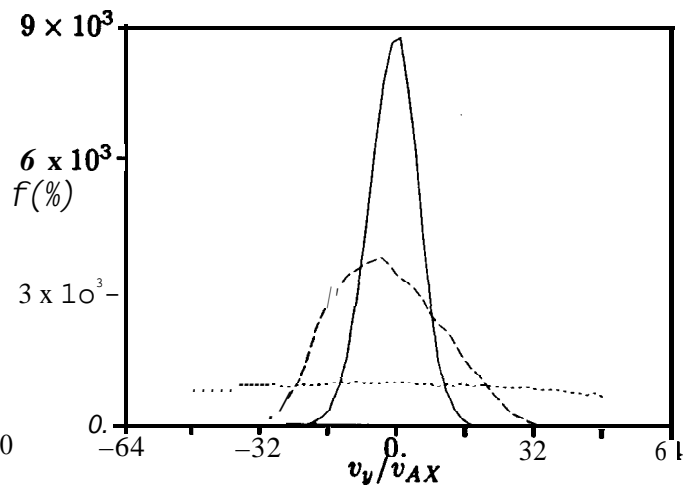
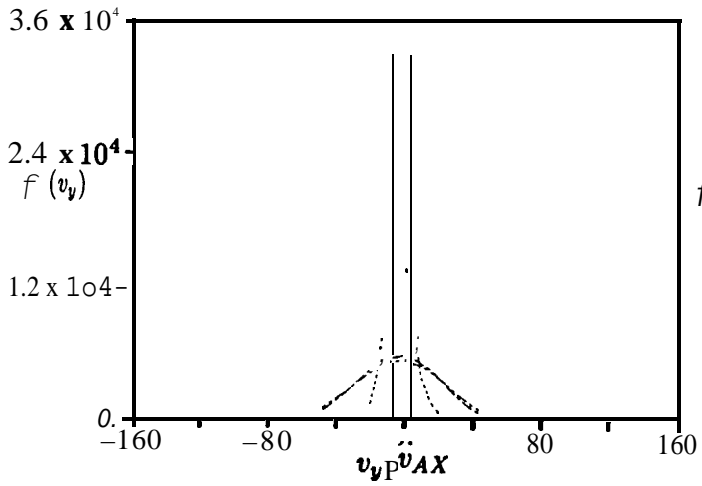
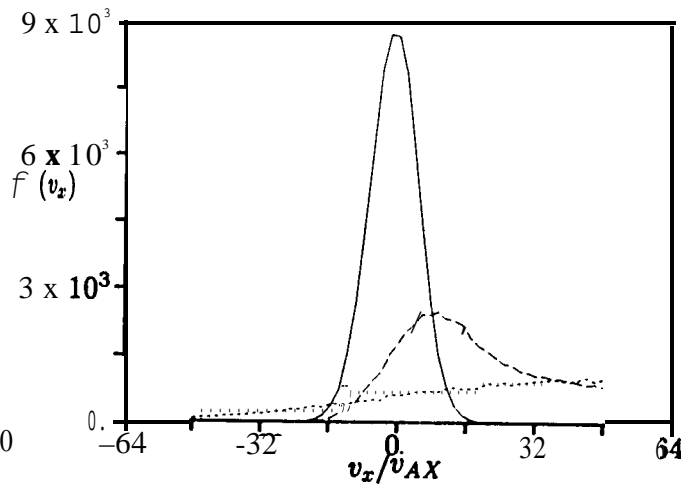
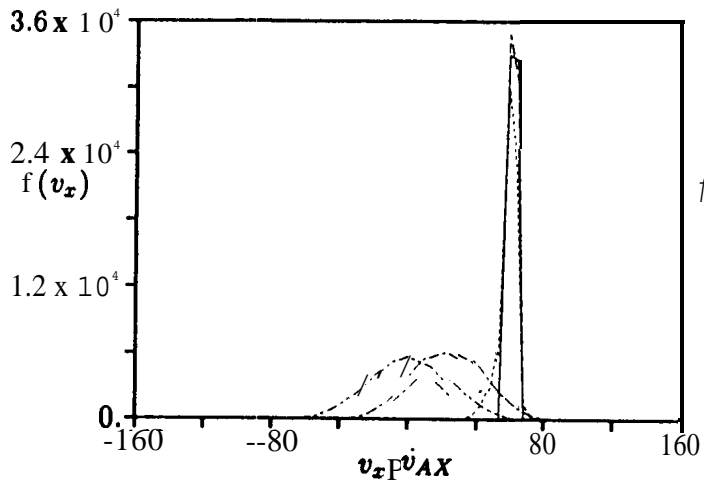


Figure 6

Figure 7

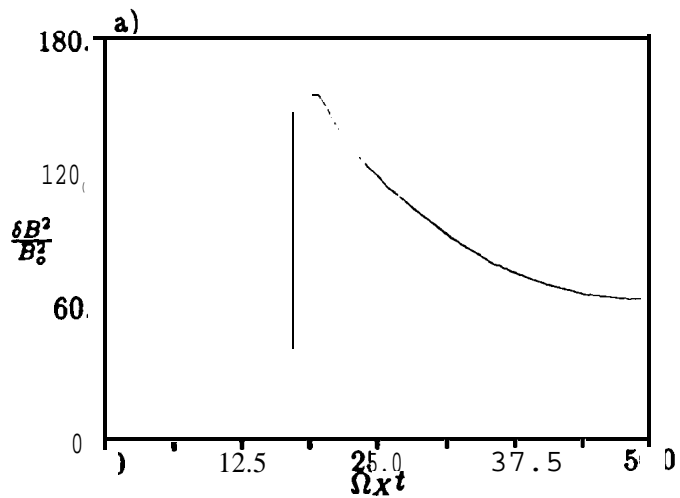


Figure 8

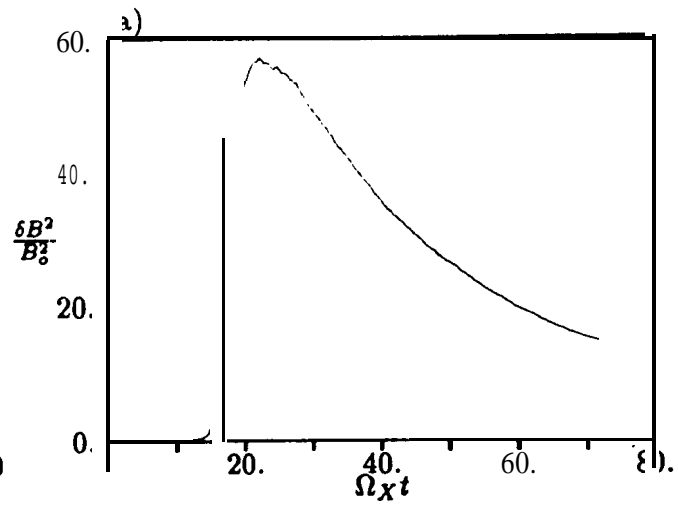


Figure 10

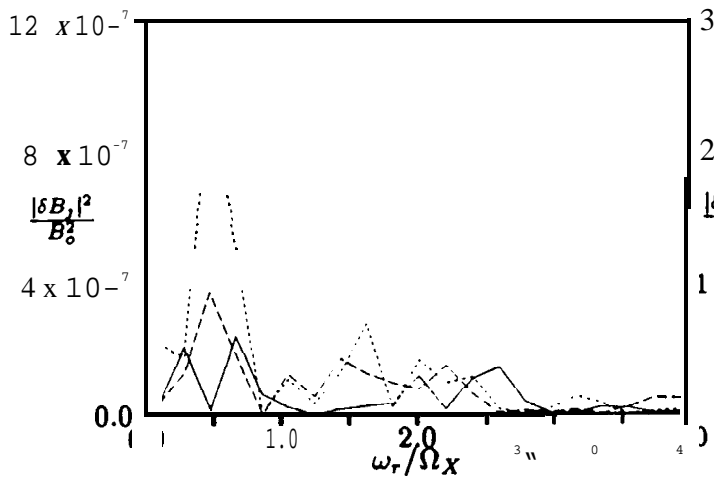
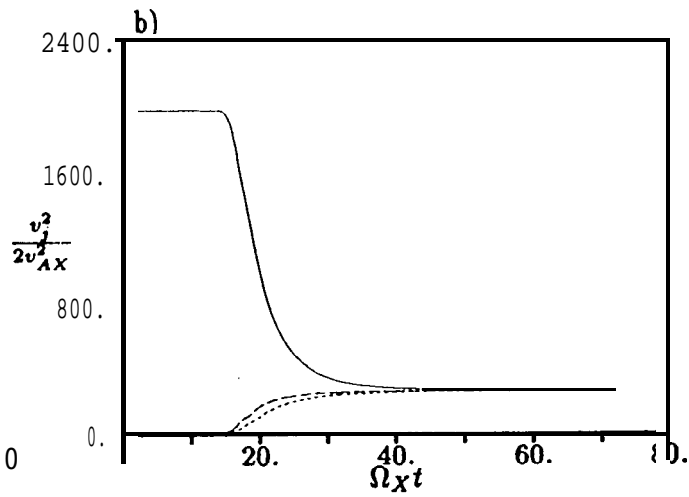
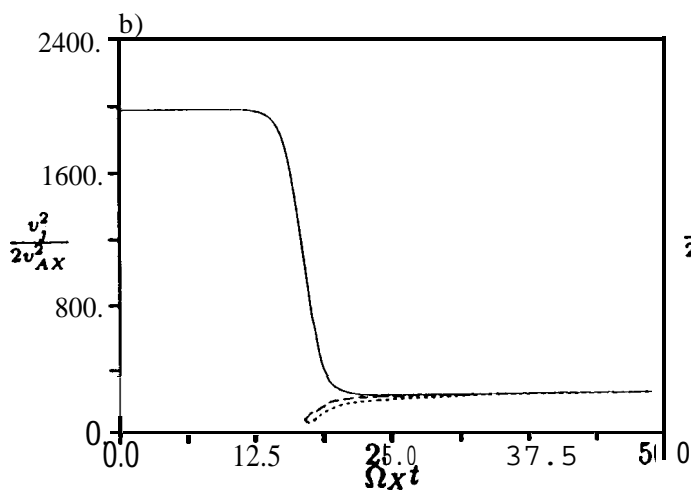


Figure 9

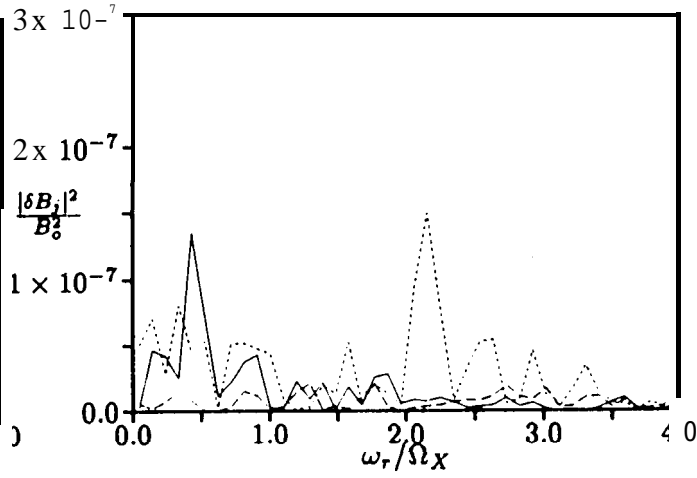


Figure 11